npj | flexible electronics

Article

Published in partnership with Nanjing Tech University

https://doi.org/10.1038/s41528-024-00303-5

Highly reliable and stretchable OLEDs based on facile patterning method: toward stretchable organic optoelectronic devices

Minwoo Nam[1,4], Jaehyeock Chang[1,4], Hagseon Kim[1], Young Hyun Son[1], Yongmin Jeon[2], Jeong Hyun Kwon[3] ✉ & Kyung Cheol Choi[1] ✉

Stretchable displays attract significant attention because of their potential applications in wearable electronics, smart textiles, and human-conformable devices. This paper introduces an electrically stable, mechanically ultra-robust, and water-resistant stretchable OLED display (SOLED) mounted on a stress-relief pillar platform. The SOLED is fabricated on a thin, transparent polyethylene terephthalate (PET) film using conventional vacuum evaporation, organic-inorganic hybrid thin film encapsulation (TFE), and a nonselective laser patterning process. This simple and efficient process yields an OLED display with exceptional stretchability, reaching up to 95% strain and outstanding durability, enduring 100,000 stretch-release cycles at 50% strain. Operational lifetime and water-resistant storage lifetime measurements confirm that the TFE provides effective protection even after the nonselective laser patterning process. A 3 × 3 array SOLED display module mounted on a stress-relief pillar platform is successfully implemented, marking the first case of water-resistant display array operation in the field of SOLEDs. This work aims to develop practical stretchable displays by offering a reliable fabrication method and device design for creating mechanically robust and adaptable displays, potentially paving the way for future advances in human-conformable electronics and other innovative applications.

In recent years, stretchable electronics have attracted significant interest for their potential in human-conformable applications, as they can be deformed into various shapes to suit diverse needs[1–8]. These versatile devices have applications across multiple domains, including sensors, photo-voltaic devices, bio-modulation therapies, semiconductors, and optoelectronics. Furthermore, advanced fabrication technologies have been instrumental in manufacturing these devices into dynamically stretchable or curved surface conformable devices[9–15].

Among these applications, stretchable displays are significant because they can revolutionize how information is accessed and engaged within everyday situations[16,17]. As a result, major efforts are presently devoted to developing practical and user-friendly stretchable displays that can seamlessly integrate with different environments. Numerous light sources have been employed in the fabrication of stretchable displays, such as alternating current electroluminescent devices, quantum dots (QLEDs), inorganic light-emitting diodes (LED), and organic light-emitting diodes (OLEDs). OLEDs are considered attractive because of their lightweight nature, efficient and harmless light emissions, thin device structure, and flexible components, which make them suitable for commercial applications such as curved monitors, foldable phones, and rollable televisions[17–19]. Moreover, the versatility of OLEDs has enabled their application to substrates, such as fibers, patches, and textiles[20–25]. It is anticipated that OLEDs' deformable capabilities will fulfill the demands of next-generation stretchable displays.

To enhance user experience, portability, and real-time information accessibility, human body conformity is considered a critical aspect of stretchable displays[26,27]. For wearable applications, these devices must be

[1] School of Electrical Engineering, Korea Advanced Institute of Science and Technology (KAIST), Daejeon 34141, Republic of Korea. [2]Department of Biomedical Engineering, Gacheon University, Seongnam 13120, Republic of Korea. [3]School of Semiconductor Engineering, Chungbuk National University, Cheongju 28644, Republic of Korea. [4]These authors contributed equally: Minwoo Nam, Jaehyeock Chang. ✉e-mail: love6539@cbnu.ac.kr; kyungcc@kaist.ac.kr

able to withstand large strains of up to 50% without mechanical failure or loss of conductivity, and they should possess a reliable structure capable of enduring repeated stretching[28–30]. Additionally, water-proof operation is crucial to ensure washable characteristics, which is a vital feature for wearable displays that may be exposed to moisture or need regular cleaning to maintain hygiene and functionality[31–33]. To address these challenges, researchers have proposed various strategies to develop highly stretchable and dependable displays utilizing OLEDs.

One such approach to fabricate stretchable OLED (SOLED) involves the use of intrinsically stretchable materials for all display elements, employing hyper-elastic substrates, conductive and stretchable nanomaterials electrodes, and polymer emissive materials[34–37]. This method yields thin, highly stretchable devices through a simple solution-based process. However, it also has issues, such as the poor stability of solution-based materials and conductive loss under stretching motion. Furthermore, integrating an encapsulation barrier into the intrinsically stretchable device is challenging, resulting in a short lifetime for the OLED.

An alternative strategy involves generating wavy patterns on OLED devices by attaching them to pre-stretched substrates and then releasing the substrates[38–40]. The wavy patterns store in-plane compressive strain energy through out-of-plane deformation, thus providing the device with stretchability. While this type of stretchable display exhibits dependable performance under multiple stretching cycles, it has difficulty maintaining uniform light emission on the light-emitting surface. Efforts have been made to develop distortion-free SOLEDs with micro-wrinkles that are imperceptible to the human eye[41]. However, forming uniform patterns on thin film devices remains a complex process that requires further innovation for practical display production.

Pioneering endeavors have been dedicated to incorporating stretchability into OLEDs. However, these attempts face obstacles, primarily concerning device stability and fabrication. Extensive studies in the stretchable electronics field have focused on patterning electrodes into geometrically stretchable configurations. This approach involves forming functional areas on islands and connecting them via stretchable electrodes. Such an island-interconnection structure is mounted on a stress-relief platform, such as pillar arrays[42], bilayers[43,44], square prisms[45], or stress-absorbing nano-fibers[46], designed to mitigate the stress from the stretching platform transfers to the functional area.

A shift in approach leads to a third strategy, where the OLED device is positioned on an elastic platform. This platform features OLED pixels on islands and interconnected by stretchable electrodes[42–44]. In such hybrid platform approaches, only the stretchable electrodes participate in the stretching motion, while the deformation of the islands is minimized. As the stretchable platform elongates, stress is transferred to the undeformed pixel islands; therefore, the islands are mounted on a stress-relief platform to prevent the brittle OLED layers from stress failure. The interconnections in these stretchable displays utilize serpentine-shaped electrodes on an SU-8 photoresist substrate or micro-cracked metals embedded within a polymer network. The OLED device is then formed on a patterned substrate using vacuum evaporation. This approach achieves stable optoelectronic performance comparable to OLEDs on glass substrates by utilizing conventional OLED materials and vacuum deposition techniques. Moreover, the stretchable device structure, which does not require a pre-stretching process, simplifies the manufacturing steps. Nevertheless, despite exhibiting some stretchability, the electrodes on the brittle SU-8 substrate and the micro-cracked metals diffused into the polymer network remain susceptible to mechanical failure, limiting the overall extent of the interconnections' stretchability. Additionally, since the patterning process using photolithography requires multiple steps and is material-dependent, the fabrication procedure becomes increasingly complex.

Previous studies have successfully demonstrated the concept's feasibility and marked significant progress in hybrid stress-relief platforms. However, these studies have yet to extensively explore the formation of pixel matrices for driving SOLEDs as display devices. Pre-patterned SOLEDs require narrowly patterned electrodes, demanding sub-micron precision for aligning fine metal masks. This precision requirement often leads to alignment challenges, potentially causing unintended light emission in the bridge areas and elevating short-circuit risk due to the current concentration in narrow areas. Moreover, uniform thin film deposition via thermal evaporation on unevenly patterned substrates poses a challenge in SOLED fabrication, primarily due to the shadow effect. In this process, vaporized materials move in a straight path, but raised features on the substrate create 'shadows,' blocking the vapor. This results in reduced material deposition on the sidewalls of SOLED structures. The shadow effect thus not only complicates the fabrication process but also significantly affects the performance and reliability of the final device. Post-patterning the substrate after the deposition process offers a solution to these issues, enabling the realization of reliable SOLEDs.

Laser cutting processes have gained prominence in fabricating stretchable electronics and enable precise and quick patterning[47–49]. By programming stretchable patterns through laser cutting, researchers can optimize the mechanical properties of stretchable devices, improving their flexibility, durability, and overall performance. Kim et al. [50] utilized selective laser patterning to tune the folding radius of the device and realized three-dimensional foldable QLEDs. Moreover, laser cutting can be easily integrated with other fabrication processes, such as lamination process, further enhancing its potential for producing electrically and mechanically robust stretchable displays[51]. The versatility of laser cutting allows for the precise patterning of multilayers composed of various materials, including oxides, metals, and polymers, making it a suitable method for post-patterning the SOLED display.

While promising strides have been made in stretchable electronics in terms of functionality and stretchability with laser patterning process, significant obstacles remain when focusing on OLED displays. Specifically, the key hurdles include preserving optoelectronic performance consistency and assuring the long-term stability of organic emissive materials. These demands have led to developing a delicate multi-layer device structure, which poses significant challenges when transitioning OLEDs into stretchable configurations. Organic layers and metals in OLEDs are highly susceptible to even ambient oxygen and moisture levels, limiting the use of wet patterning methods during fabrication. Such highly reactive constituents require encapsulation that exhibits low water and oxygen permeability and possesses chemical resistance. However, it is essential to note that the encapsulation layer shields the OLED from ambient conditions and is not designed to endure further chemical processing. The encapsulation layers add another level of complexity to the fabrication process, substantially curtailing the efficiency of selective wet or dry patterning. Moreover, the brittle encapsulations based on inorganic layers, which can only withstand a mechanical strain of less than 1%, are widely seen as a bottleneck to achieving high stretchability. While neutral axis engineering is often employed in flexible OLED displays to alleviate strain on the encapsulation, its application to real SOLED displays is difficult to utilize because all elements are stretched simultaneously. Therefore, in a situation where no stretchable encapsulation film can guarantee the reliability of OLED in terms of material and structure, the most realistic method is to develop it so that mechanical stress is not applied to the encapsulation film by mechanical stretching[52].

This paper presents a facile fabrication method of highly reliable SOLED on a stress-relief pillar platform to overcome issues raised in previous SOLED research. The SOLED is fabricated on a thin, transparent polyethylene terephthalate (PET) film using conventional vacuum evaporation, organic-inorganic hybrid thin film encapsulation (TFE), and nonselective laser patterning to create an island-interconnection structure. SOLEDs were realized through a post-process of substrate patterning after the completion of OLEDs and encapsulation films. This strategy facilitated the creation of pixelated OLEDs, enhancing the device's overall performance and visual quality. This streamlined fabrication method yields an electrically stable device with performance comparable to traditional OLEDs on glass substrates. The SOLED demonstrates ultra-robust mechanical performance, achieving a maximum strain of 95% and enduring 100,000 stretch-release cycles at 50% strain. Moreover, the device boasts

a robust operational lifetime of 753 h before 60% degradation at an initial luminance of 1000 cd·m^{-2} and a water-resistant storage lifetime exceeding one month, verifying the effectiveness of the TFE in protecting the SOLED even after laser patterning. A 3 × 3 SOLED array mounted on a stress-relief pillar platform successfully demonstrated display operation and water-resistant capabilities. This work aims to advance the field of stretchable displays by offering reliable solutions for creating highly adaptable and mechanically robust devices, paving the way for human-conformable electronics and a range of innovative applications beyond.

Results

The procedures illustrated in Fig. 1a enable a simple and straightforward fabrication of the SOLED. Bottom-emitting OLED devices are formed using conventional vacuum evaporation and are fully encapsulated with TFE on a resilient and transparent PET film (12μm). The encapsulation barrier is comprised of 3.5 dyads inorganic-organic hybrid TFE, featuring four nano-stratified layers of Al_2O_3 and ZnO formed through atomic layer deposition (ALD), as well as three SiO_2 polymer layers deposited via spin-coating[53,54]. Following the deposition process, an attachable PET film (12μm) is applied to the device surface as a top cover through a lamination process. This top cover positions the OLED device within the neutral axis (NA) plane and protects it from physical damage. Subsequently, the device is aligned and patterned using a CO_2 laser cutting process (Universal VLS 3.50), resulting in a SOLED composed of light-emitting islands and stretchable electrode interconnections. The electrodes are patterned into a Kirigami structure, a design widely utilized in stretchable electronics due to its symmetric and large axial motion capabilities[55,56].

The patterning process for stretchable structures has been a major challenge for geometrically SOLED displays. The patterning method determines the substrate material and the complexity of the procedure, affecting the device's stretchability and electrical performance[16]. To employ a laser cutting process to fabricate SOLED displays, this work uses a plastic film, specifically PET, as the display substrate. The ductile mechanical properties of PET help prevent substrate structure failure beyond the yield strain point (Supplementary Fig. 1), allowing the device to reliably endure large deformations, which will be analyzed later.

Previous studies on SOLED displays using interconnection structures employed photoresist substrates (SU-8), which had to be selectively patterned by photolithography[42,43]. Consequently, complex fabrication steps, such as substrate patterning, lift-off, transfer, and alignment processes, have been required prior to OLED evaporation. In contrast, this work employs nonselective patterning using laser cutting, which simplifies the fabrication procedure. Although selective patterning processes, such as wet and dry etching, could be candidates for patterning the substrate, traditional wet or dry etching methods exhibit selective behavior, making it nearly impossible to optimize the etching process for several multilayers in an OLED device. Furthermore, etchants or gases used in etching can damage the OLED structure, diminishing its performance and stability. The complete fabrication process is detailed in the Supplementary Information. (see Supplementary Fig. 2) According to the proposed procedure, the OLED device is formed on a planar PET film using a conventional flexible OLED fabrication method[55–57]. After the OLED fabrication, the device is aligned and patterned by a laser cutter, which simultaneously ablates the plastic film, metallic electrode, and TFE layers.

Figure 1b presents detailed schematics of an OLED island in an exploded view, which illustrates the device structure. The OLED device is formed between PET films and encapsulated top and bottom by TFE. The composing layers of the device include the bottom transparent anode (Ag, 30 nm), active layer, and top cathode (Al, 100 nm). Laser paths are programmed to pattern the electrodes around the island into Kirigami configurations. The Kirigami structure was chosen for patterning the interconnection due to its inherent advantage of imparting stretchability through simple line cuts. In terms of cutting trajectories, Kirigami designs tend to have shorter, more direct cuts compared to the serpentine structures' lengthy and winding patterns. This difference can lead to several advantages regarding manufacturing efficiency and reduced tact time when using the laser patterning process. Also, the Kirigami structure's ability to transform an in-plane sheet into an out-of-plane structure through a series of cuts provides superior stretchability compared to traditional design approaches[58–60]. Depending on the electrode material applied to the structure, a Kirigami-based electrode can be used as a strain-sensitive or a strain-resilient electrode. Its application has been demonstrated in various state-of-the-art devices, like gas sensors[61,62], health monitoring electronics[63,64], electrodes[58], and batteries[65,66], improving their mechanical robustness while maintaining functionality.

For nonselective patterning, the device layout must consider the material's response to laser ablation. Notably, the selection of metals for nonselective patterning is crucial due to varying laser ablation thresholds. As Kim et al. reported[50], metals such as Ag, Au, and Cu, characterized by higher ablation thresholds, require more energy for effective etching. High energy ablation increases the width of the cut line due to Gaussian energy dispersion of the laser beam[67] and risks extensive thermal damage to the device. On the other hand, metals like Al, Ni, and Fe have low ablation thresholds, making them more suitable for precise and efficient patterning. These metals necessitate less energy for ablation, thereby minimizing damage to the multi-layer structure and reducing the heat-affected zone.

In this work, transforming the electrode interconnections into a Kirigami structure involves laser cutting through the metal layers, with Ag and Al as candidates. The Kirigami cuts, strategically implemented at the electrode structure, are designed to preserve electrical conductivity between the stretching interconnection and the active OLED area, simultaneously facilitating controlled stretching and bending of the device. Figure 1c shows that the laser cutter successfully removed all layers of the Al electrode interconnection while failing to cut through the Ag electrode interconnection at the laser power of 3.2 W with 350 pulses per inch (PPI). Although the interconnection consisting of an Ag electrode can also be patterned with higher laser power, the cut line becomes wider (Supplementary Fig. 3), and the interconnection suffers more thermal damage. Therefore, the device's electrodes should be arranged so that laser paths ablate the Al layer while avoiding the Ag layer.

As shown in Fig. 1d, adding wings to the Ag anode layout resolved the issue. The bottom view of an OLED island illustrates the device layout, consisting of a scan line in a row and a data line in a column. The scan line comprises a continuous Al layer, while the data line consists of separated Al interconnections and an Ag island. Short, narrow wing structures protruding from the Ag island establish metal-to-metal contact with the Al interconnections, completing the data line. This layout clears the Ag layer out of the laser paths and provides Al layers for both scan and data line electrodes. (Supplementary Fig. 4).

Figure 1e demonstrates a 3 × 3 array of SOLEDs and a magnified view of a Kirigami interconnection fabricated by an optimized nonselective laser cutting process. The device consists of square islands with a 12 mm pitch, a 5 × 5 mm square active area, and Kirigami interconnections with a nominal length of 5.4 mm. The cut lines for the Kirigami interconnection are created by one-way laser beam travel, resulting in a cut line thickness of 0.15 mm. Due to the Gaussian energy dispersion of the laser, round fillets with a diameter equal to the cut line thickness are formed at the vertices of the cut lines.

To evaluate the optoelectronic performances, red, green, and blue 2 × 1 array unit SOLEDs were fabricated. Figure 2a shows the bottom emission structures of the phosphorous red, fluorescent green, and blue OLEDs used for the evaluation. They had peak wavelengths of 621 nm, 527 nm, and 468 nm, respectively, as plotted in Fig. 2b. Detailed information about the materials is explained in the experimental section.

The SOLED substrate features 3.5 dyads of organic-inorganic barrier layers, which protect against oxygen and moisture infiltration and create a smooth surface. When applied to the PET substrate of the SOLED, these barrier layers result in a surface with low roughness, comparable to both a bare glass substrate and the same barrier layers on a glass substrate.

The current density-voltage-luminance (JVL) measurements show that the optoelectronic performance of the SOLED is as stable as OLEDs

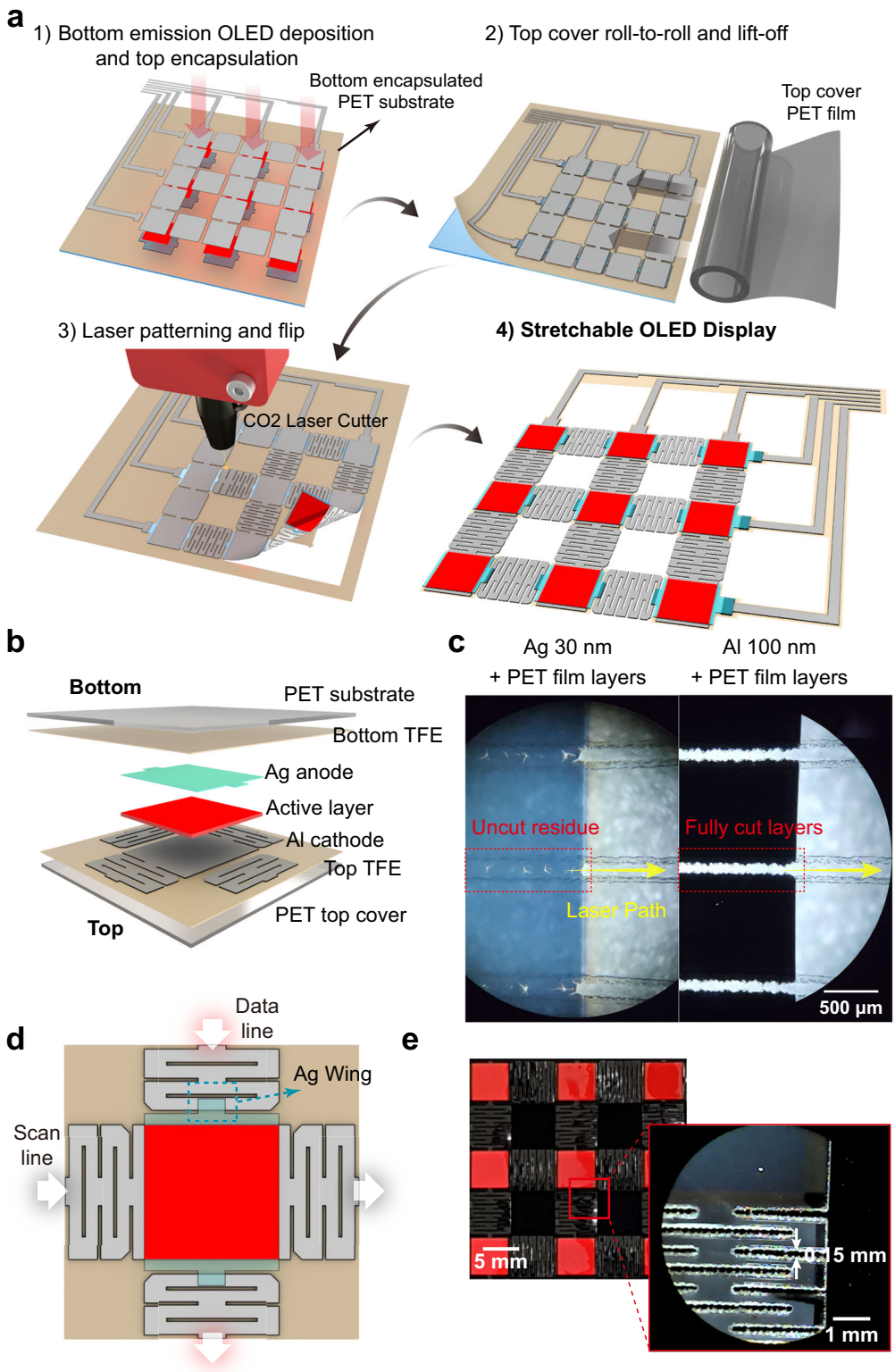

Fig. 1 | SOLED display concept and fabrication. a Schematic representations of the SOLED fabrication process. **b** Exploded view of a SOLED pixel. **c** Laser ablation parameters on interconnections made of 30 nm Ag and 100 nm Al layers, sandwiched between 12 μm PET film layers. **d** Top view of a SOLED pixel. **e** Operating SOLED photo with a magnified view of a Kirigami interconnection.

formed on glass substrates. For experimental comparison, OLEDs were fabricated in three cases: (i) on a bare glass substrate without encapsulation (Bare Glass Ref), (ii) with bottom and top TFE on a glass substrate (Encap. on Glass), and (iii) as SOLED. (Supplementary Fig. 5) Fig. 2c, d, and e displays images of the operating 2 × 1 array unit red, green, and blue (RGB) SOLEDs, respectively. Figure 2f, g, and h display the JVL curves for the RGB OLEDs, while the current efficiency curves are shown in Fig. 2i, j, k. For the red SOLED, electroluminescence was turned on at a voltage of 2.25 V, the

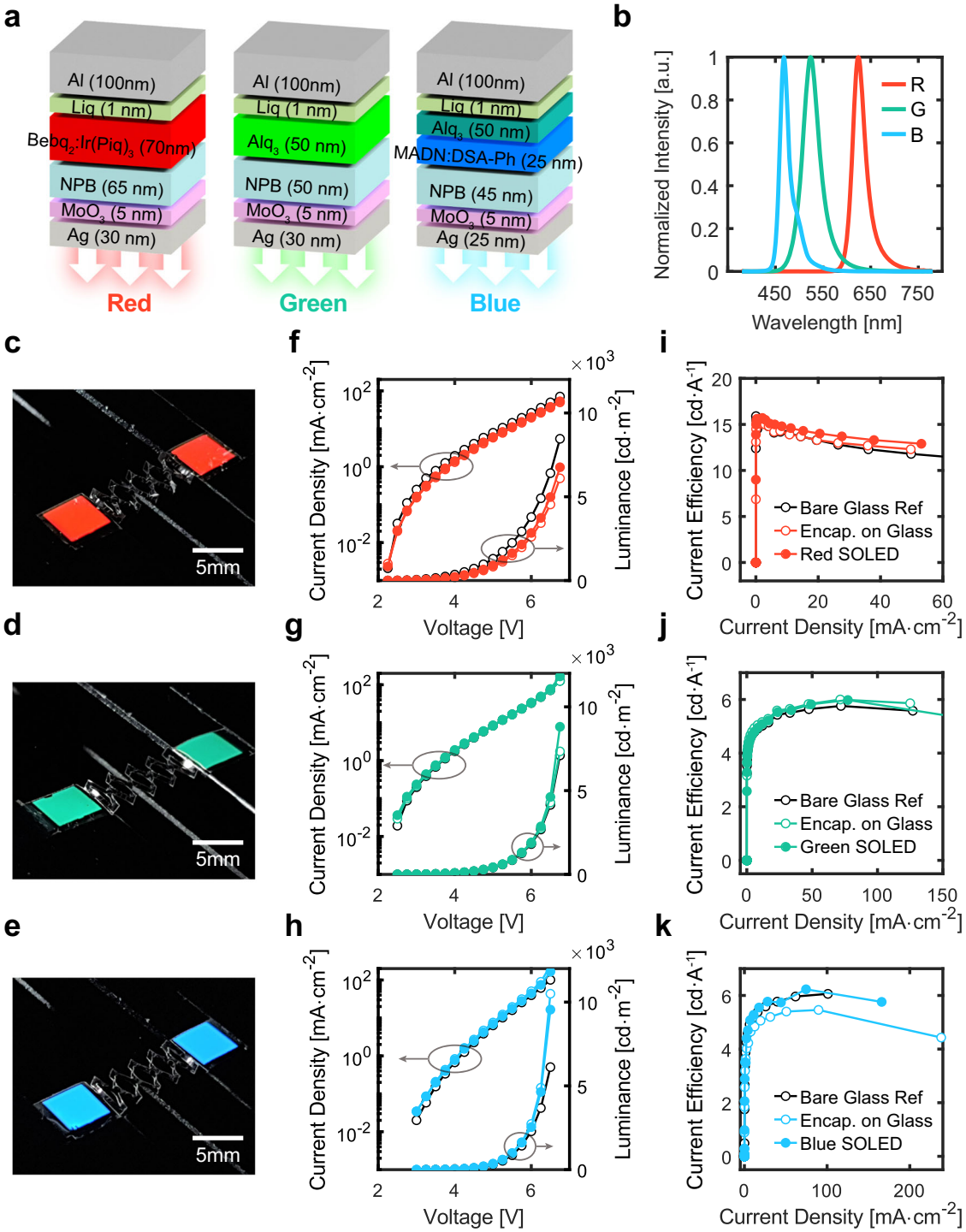

Fig. 2 | Device characteristics of the SOLEDs. a Bottom emission structures for red, green, and blue SOLEDs. **b** Spectra for the fabricated RGB OLEDs. **c**, **d**, **e** Operating images of unit RGB SOLEDs, **f**, **g**, **h** J-V-L curves, and **i**, **j**, **k** current efficiency to current density curves for red OLEDs in three fabrication scenarios: Bare glass substrate without encapsulation (Bare Glass), Glass substrate with bottom and top TFE (Encap. on Glass), SOLED configuration.

same as both the bare glass substrate and encapsulated glass substrate cases. The maximum current efficiencies were within a narrow range of 15.2–15.9 cd·A^{-1}, and the luminance of the OLEDs reached 1000 cd·m^{-2} at a current density of 7.5 mA·cm^{-2} in all three cases. Similarly, the JVL curves of green and blue OLEDs were comparable for all the samples. The overlapping current efficiency curves in Fig. 2c indicate no leakage current in the SOLED, demonstrating its stable optoelectronic performance.

Figure 3a demonstrates the unit SOLED being stretched by a uni-axis stretching machine from 0% to 95% strain (see Supplementary Fig. 6 for all photos of stretching motion). Here, the system strain ε_s of stretching motion, which will be simply referred to as strain in this study, is defined as follows.

$$\varepsilon_s = \frac{\Delta l}{l_0}(\%) \tag{1}$$

Δl is the length change, and l_0 is the pitch of the unit SOLED. As the device stretches, the Kirigami interconnection transitions into an out-of-

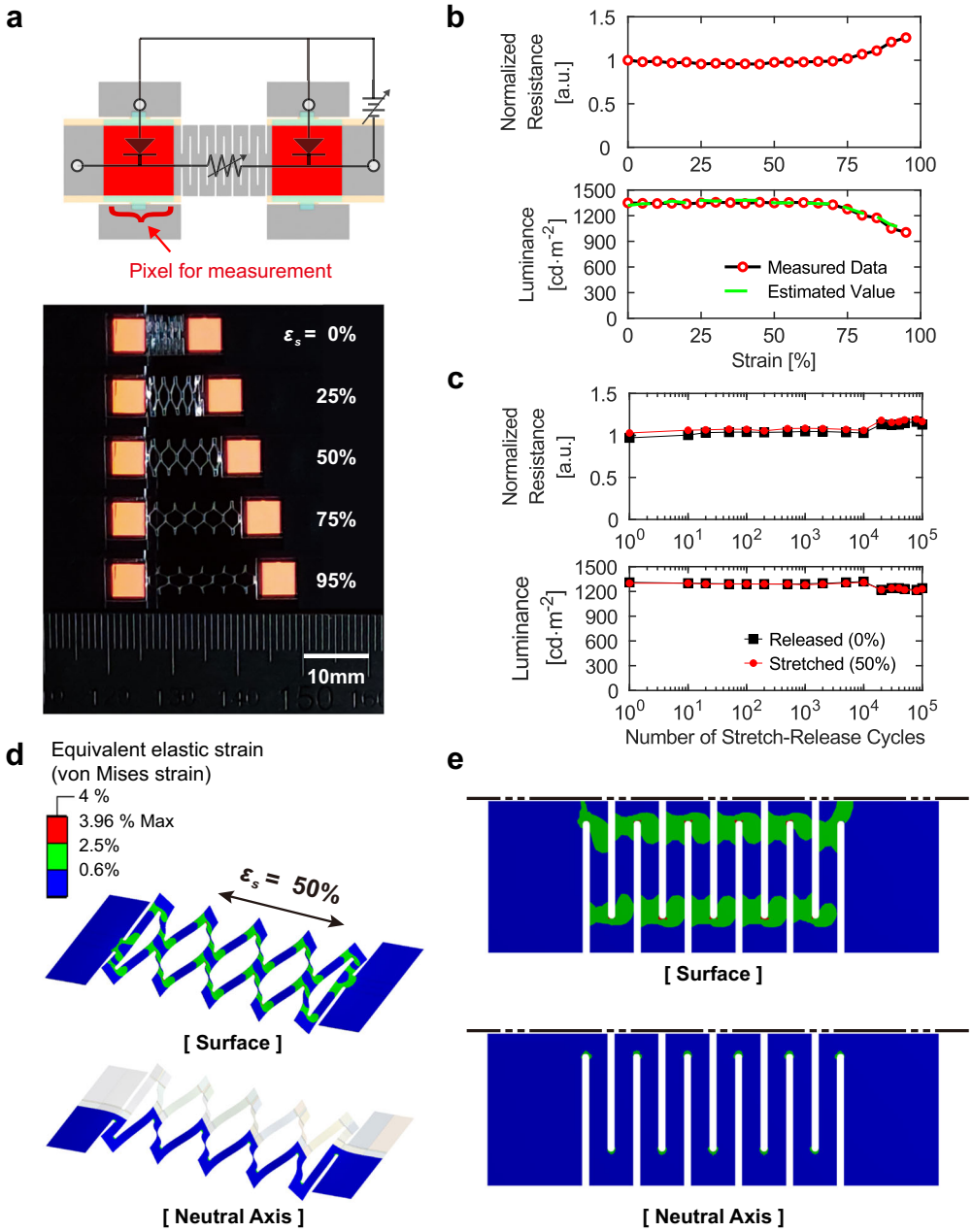

Fig. 3 | Stretching test and FEM simulation results of a unit SOLED. a Circuitry setup for a unit SOLED to evaluate the impact of interconnection deformation on optical performance, with images of an operating unit SOLED under gradual stretching up to 95% strain. **b** Normalized resistance and luminance of the SOLED during incremental stretching of 5% strain. **c** Normalized resistance and luminance of the SOLED during 100,000 cyclic stretching tests at 50% strain. **d** FEM results highlighting Kirigami interconnection at 50% system strain, presenting equivalent elastic strain (von Mises strain) for both surface and neutral axis. **e** Detailed FEM result depiction with the structure in an undeformed configuration for clarity.

plane configuration as cut lines spread apart. The mechanical durability of the Kirigami interconnection was assessed by stretching the unit SOLED, as shown in Fig. 3a. This setup enables observation of the impact of electrode deformation on a pixel of interest, as the circuitry incorporates the interconnection as a variable resistor. A typical OLED exhibits a linear relationship between current density and luminance. Thus, a relationship can be established between luminance and normalized resistance.

$$L = \frac{\eta \cdot V}{A \cdot R_i \cdot R} \tag{2}$$

In the relationship, L is the luminance, η the current efficiency, V is the voltage potential, A is the active area of the pixel, R_i is the initial resistance, and R is the normalized resistance. The relationship is a simplified model of the system, considering that only the resistance of the electrode varies, and the current efficiency is constant. Details of the relationship are presented in the Supplementary Information (see Supplementary Fig. 7).

The mechanical tests of the SOLED showed that it can withstand 90% strain and remain operational after 100,000 cycles of 50% strain stretching. Initially, the normalized resistance and luminance were measured from 0% to 95% strain in increments of 5% (Fig. 3b). The unit SOLED was driven with a constant 5 V, generating 1000 cd·m^{-2} at 0% strain. Both indicators exhibited negligible changes up to 70% strain. The increase in normalized resistance began at 75% strain, withstanding a maximum strain value of 95%. Luminance showed an inversely proportional relationship with the normalized resistance. The dashed green line in Fig. 3b represents the

estimated luminance corresponding to the normalized resistance. Even though the relationship between luminance and normalized resistance is based on a simplified model, it yields a reasonably accurate approximation with an error margin of only 5%. The concept of maximum strain in display technology differs from maximum stretchability, which refers to the device's endurance limit. From a display perspective, maximum strain is defined as the point at which a change in luminance becomes perceptible to the human eye, typically at a 5% variation[68,69]. This threshold of visual perception is crucial for maintaining display quality under strain. As illustrated in Fig. 3b, this definition aligns with the point where a 5% change in resistance is observed, marking the maximum strain level. This 5% resistance change corresponds to approximately 78% strain on the electrode. Further, a cyclic stretch and release test was conducted to investigate the SOLED's mechanical durability. The sample was repeatedly stretched to 50% and released to 0% at a speed of 1200 mm·min^{-1}, corresponding to a strain rate of 167% per second. The normalized resistance and luminance were then measured before (0% strain) and after stretching (50% strain) at a constant voltage of 5 V.

Further, a cyclic stretch and release test was conducted to investigate the SOLED's mechanical durability. The sample was repeatedly stretched to 50% and released to 0% at a speed of 1200 mm·min^{-1}, corresponding to a strain rate of 167% per second. The normalized resistance and luminance were then measured before (0% strain) and after stretching (50% strain) at a constant voltage of 5 V. As plotted in Fig. 3c, resistance increased by up to 10% while luminance degradation was within only 3% until 10,000 cycles. Additionally, until 100,000 cycles, the maximum increase in resistance compared to the initial resistance remained within 22%, while the decrease in luminance was within 10%. These results demonstrate the mechanical robustness of the SOLED, which is the most enduring SOLED reported to date.

NA engineering is a crucial factor to ensure the mechanical robustness of Kirigami interconnections. Kirigami interconnections stretch in the in-plane direction due to consecutive out-of-plane bending of the structure[47,70]. During bending deformation, the interconnection structure experiences larger strains at the outer planes subjected to compression or tension, while an NA exists where strain is minimal or theoretically zero. Applying a top cover PET film through a lamination process, the encapsulation barrier and electrode layer are strategically placed at the NA between the PET substrate and the top cover. As a result, NA engineering enables the ductile PET film to withstand large strains while the brittle layers encounter minimal strain.

The effect of NA engineering was investigated using the finite element method (FEM) via ANSYS static structure simulation. The interconnection structure consists of a PET film with a Young's Modulus of 4.4 GPa and a Poisson's ratio of 0.43. The structure was modeled with a SOLID 186 and 187 elements in ANSYS Workbench, and its stretching motion was solved using a large deflection solver. Figure 3d displays the equivalent von Mises strain results for the outer surface and the NA planes of the Kirigami structure between two islands under 50% strain, respectively.

The electrical failure of the interconnection at 100% strain was primarily due to crack propagation within the electrode layer. The cracks originated at the edges of the cut line, where the strain was highest, and then progressed, eventually leading to the breakdown of the electrode layer. Simulation results depicting the neutral axis plane reveal how the strain propagated as the interconnection deformed from 50% to 100% strain (see Supplementary Fig. 8). Notably, the failure of the electrical connection was attributed to the fracturing of the electrode layer rather than to substrate material failure. Although the interconnection exhibited permanent deformation beyond 95% strain due to plastic deformation, the ductile properties of the PET substrate averted a complete substrate material failure, thus contributing to the overall stretchability of the structure.

Low strain (below 0.6%) is observed at the bending bridges, while moderate strain (0.6–2.5%) is concentrated near the hinges. In the moderate strain range, the encapsulation and electrode layers could fail, but the PET film undergoes elastic deformation. When the entire structure is stretched to 50% strain, Fig. 3e shows moderate strain across a large portion of the interconnection surface plane, yet the strain is localized to a limited area at the hinge part near the NA. Positioning encapsulation and electrode layers on the NA plane minimizes the potential for interconnection failure due to cracking. Upon stretching to a system strain of 100%, the area of moderate strain extends from the hinge, which may lead to the failure of the encapsulation layer. (Supplementary Fig. 9) The simulation result is consistent with the observed crack at the hinge of the interconnection. This result highlights the strategic use of NA for enhancing the mechanical robustness of the Kirigami interconnection, achieved by employing the lamination process and nonselective laser patterning.

The SOLED, effectively encapsulated by TFE, exhibited robust performance when exposed to air and moisture. A 3.5 dyad inorganic-organic hybrid TFE was applied to both the top and bottom of the OLED, which had a commercial-grade water vapor transmission ratio on the order of 10^{-6} g·m^{-2}day^{-1} [53]. (Supplementary Fig. 10, 11) After the encapsulation process, the SOLED structure was patterned using a nonselective laser cutting process, ensuring the OLED remained unexposed to the external environment (Fig. 4a).

An operational lifetime test was conducted to evaluate the encapsulation barrier of the red SOLED. (Fig. 4b) The samples were tested in ambient air at 23 ± 2°C and 55 ± 10%RH and driven at 5.1 V for a luminance of 1000 cd·m^{-2} to evaluate their operational stability as a voltage-driven passive matrix. The operational lifetime at 60% relative luminance (LT_{60}) of the SOLED was 753 h, while the OLED on a glass substrate only survived for 104 h of LT_{60}, confirming the effectiveness of the encapsulation barrier. Additionally, the LT_{60} of the SOLED was comparable to an OLED on a glass substrate with the same encapsulation barrier, which was 810 h. This result demonstrates that the laser patterning process did not compromise the encapsulation barrier and effectively blocked the infiltration of oxygen and moisture.

To further evaluate the stable encapsulation performance under harsh conditions, the SOLED was submerged in deionized (DI) water to assess its water-resistant storage lifetime. As a reference a red OLED fully encapsulated on a glass substrate was prepared and stored to test its water resistance. During the water-resistant storage test, the SOLED was attached to a polydimethylsiloxane (PDMS) coated carrier glass to suppress buoyancy. Periodically, the samples were removed from the water to measure their luminance at 5 V. As plotted in Fig. 4c, the luminance of the SOLED and the reference samples were measured for one month, and both samples showed negligible change.

Figure 4d shows a demonstration of a unit SOLED operating in DI water. In the demonstration, the SOLED, driven at 4 V for visibility, endured stretching, tilting, and folding motions. (Supplementary Video 1) The results prove that the encapsulation barrier of the SOLED is effective even after nonselective laser patterning. Moreover, its water-proof ability confirms its potential robustness for washable and wearable SOLED applications.

Figure 5a presents a schematic illustration of a SOLED display module, which includes a 3 × 3 SOLED array mounted on a stress-relief pillar platform and connected to a microcontroller unit. The stress-relief pillar platform, made of mold-casted PDMS (Supplementary Fig. 12), helps reduce stress on the OLED device during stretching[42]. The necessity for a stress-relief structure in the interconnection arises from the Kirigami structure's behavior during stretching. The Kirigami structure rotates as it stretches to alleviate stress, resulting in out-of-plane motion. In the absence of pillar support on a flat substrate, this out-of-plane motion can exert considerable stress, potentially leading to delamination and malfunction of the device. Beneath each island of the SOLED array, a 2 × 2 cylindrical pillar array was bonded using silicone adhesive. A microcontroller unit (MCU, Arduino Uno) was connected to the SOLED via a 6-pin flexible flat cable (FFC) to enable passive matrix control. The FFC is attached to the SOLED using a layer of anisotropic conductive film (ACF) tape. The ACF tape establishes an electrical connection between the scan and data lines of the passive matrix and FFC in the vertical direction, ensuring strong adhesion and reliable electrical connection.

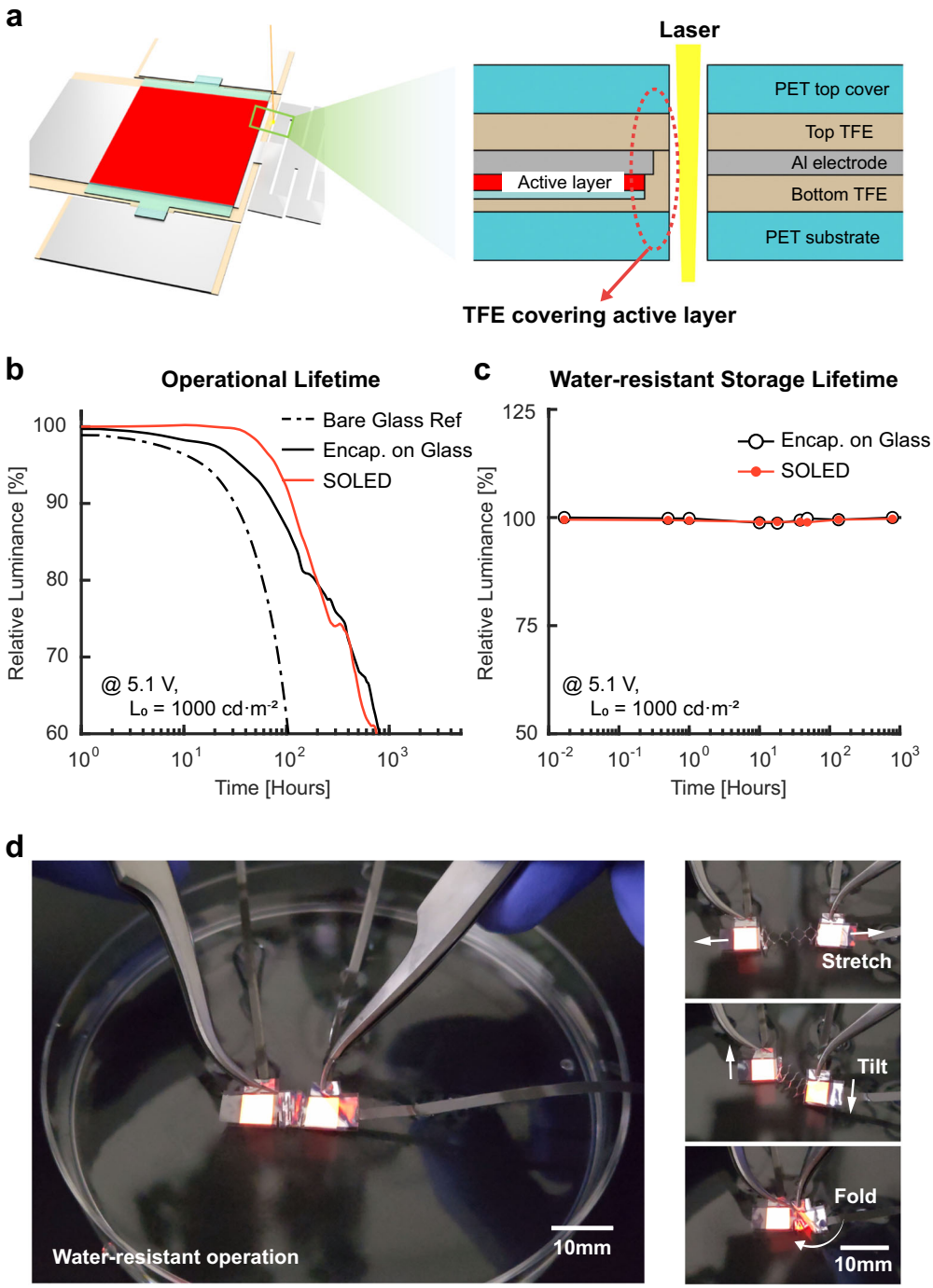

Fig. 4 | Reliability and water-resistant performance of a unit SOLED. a Cross-sectional illustration of SOLED near the pixel island, highlighting the laser path's design to preserve the TFE covering the active layer post-patterning. **b** Operational lifetime comparisons of red OLEDs fabricated under three conditions: on a bare glass substrate without encapsulation, but with a top PET cover film (Bare Glass), featuring both bottom and top TFE on a glass substrate (Encap. on Glass), and in the form of SOLED, all driven at a steady 5 V with an initial luminance of 1000 cd·m^{-2}. **c** Water-resistant storage lifetimes of Encap. on Glass and SOLED configurations, both stored in DI water for a month, with luminance measurements taken at 5 V post submersion during testing. **d** Display of a unit SOLED's functionality under water, showcasing its resilience through stretching, tilting, and folding actions. (Refer to Supplementary Video 1).

When the display module is uniaxially stretched on the pillar platform, the Kirigami interconnections in the axial direction stretch as previously analyzed. Meanwhile, interconnections in the perpendicular direction compress due to the Poisson's ratio of the platform material. As illustrated in the schematic, the Kirigami interconnection also stably endures compression due to symmetric out-of-plane buckling. During the stretching motion, the elastic pillar array in the stress-relief platform absorbs the strain energy through its deformation, effectively isolating the stress transferred from the stretched platform to the SOLED islands. (Detailed photos are presented in Supplementary Fig. 13) Fig. 5b and Supplementary Video 2 showcase a SOLED display module operating at 0% strain and extending horizontally to 50% strain.

Seamless adaptation to human body contours requires a stretchable display capable of adjusting to varying Gaussian curvature. On a surface with double curvature, the SOLED array, supported by the stress-relief pillar platform, conforms to surface curvature, stretching on surfaces with positive

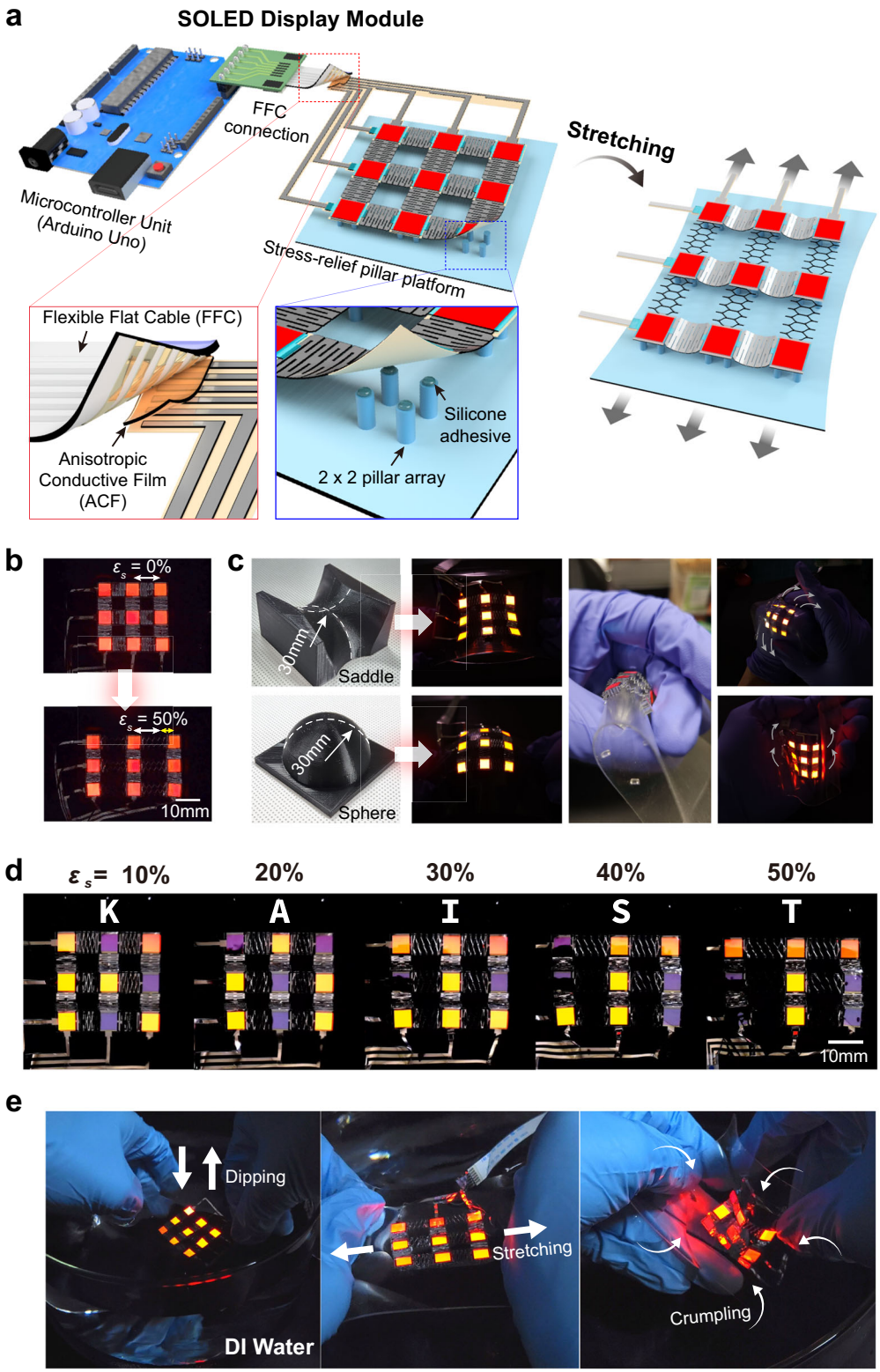

Fig. 5 | Schematic illustration and demonstration of a 3 × 3 SOLED display module. a An illustration of the SOLED display module in both relaxed and stretched configurations. **b** Depictions of the SOLED display module at both 0% strain and stretched up to 50% strain. **c** Demonstrations of the SOLED display module conforming to various surfaces, including a dual-directional curvature saddle with 30 mm radii and a 30 mm radius hemisphere. The module remains operative on a tightened human fist and when crumpled onto a hand. **d** Displays of the SOLED display module presenting the word 'KAIST', undergoing stretching in 10% increments, culminating at 50% strain by the final letter 'T'. **e** Displays of the SOLED module operating in the water, illustrating resilience to dipping, stretching, and crumpling motions while submerged.

curvature and compressing on those with negative curvature. As demonstrated in Fig. 5c, the SOLED array was applied to both a saddle shape and a hemisphere, and each was created using additive manufacturing (3DWOX1, Sindoh Co.). The saddle features opposing curvatures across two principal directions, each with a radius of 30 mm, contrasting the hemisphere's uniform curvature with the same radius. The results showcase the SOLED array smoothly adapting to these surface contours while operational. Further application of the SOLED display array was demonstrated on a human fist and under the condition of crumpling onto a human hand, indicating its potential for conforming to dynamic human motion and body contour.

Figure 5d and Supplementary Video 3 show the SOLED sequentially displaying the word "KAIST". Starting with the letter "K" at 10% strain, the display module stretches in 10% increments, reaching 50% strain at the letter "T". The SOLED display was driven using a line-scanning method at 5 V by an MCU. In the demonstration of Fig. 5, the color variance between the pixels is observable due to the microcavity structure of the OLED utilized in this work. The microcavity effect causes the color shift depending on the viewing angle, as explained in Supplementary Fig. 14 of Supplementary Information. These color differences are primarily attributed to the influence of the microcavity structure on the viewing angle, a situation further intensified by the camera's close placement. The camera was placed close to the display module to capture detailed images of the stretching SOLED under low light conditions, inadvertently creating larger viewing angles.

Supplementary Fig. 15 shows the stretching display module with significantly less color variance since its image is captured at a greater distance. Additionally, Supplementary Fig. 16 presents the luminance and spectrum of the stretching SOLED display module. The data presented in Supplementary Fig. 16a, acquired using a spectro-radiometer aligned perpendicular to a pixel driven at a constant 5.1 V for an initial luminance of 1000 cd/m², reveals that the luminance of the display module remains consistent up to 70% uniaxial strain. Moreover, the spectrum of the SOLED pixel, as depicted in Supplementary Fig. 16b, is maintained throughout the stretching.

The water-resistant performance of the SOLED display, previously tested with a unit SOLED, was further demonstrated. Figure 5e shows a 3 × 3 array SOLED display submerged in DI water and driven using a 5 V line-scanning method by an MCU. The display demonstrated its washable capabilities and adaptability to various motions as it was dipped, stretched, and crumpled in water. (Supplementary Videos 4, 5) Throughout the water-resistant operation, no dark spots or OLED degradation were observed. This is the first demonstration of water-resistant display operation to date. Also, the performance and reliability of the SOLED display presented in this work surpass those of previous studies, as detailed in Table 1. For more discussion, the advantages and limitations of the methodology proposed in this study are comprehensively summarized in Supplementary Table 1 of Supplementary Information, contrasted with prior research for comparative analysis. By exhibiting stretchability and water-resistant performance, the SOLED display presented in this work exemplifies the potential for a truly robust and practical display solution for wearable technologies.

Discussion

This work presents an ultra-robust and water-resistant SOLED fabricated with a simple and efficient process. Utilizing nonselective laser patterning, SOLEDs were produced by conventional processing on a PET substrate, combined with the straightforward application of TFE and lamination processing of a top cover PET film. The fabrication method introduced in this work effectively addresses common challenges in SOLEDs, such as achieving stable optoelectronic operation and designing mechanically robust structures to accommodate large stretchability and high reliability. The PET substrate, with a well-planarized surface morphology facilitated by 3.5 dyads of TFE, resulted in SOLED electroluminescent performance comparable to OLED devices fabricated on glass substrates. Furthermore, the integration of lamination processing and nonselective laser patterning enabled effective NA engineering in the device. This approach successfully produced Kirigami interconnections and OLED islands with large stretchability, superior mechanical robustness, and device reliability, capable of operating even when submerged in water.

Consequently, a 3 × 3 SOLED display module was demonstrated. Mounted on a stress-relief pillar platform, the SOLED display module exhibited stable passive matrix operation while stretched to 50% strain and excellent water-resistant performance, maintaining its integrity and functionality during various underwater motions. These advances in both stretchability and water resistance are anticipated to enable the development of practical stretchable displays. Such displays hold great potential for applications in wearable electronics, smart textiles, and human-conformable devices that can withstand real-world usage and diverse environments.

Methods

PET substrate preparation

A thin layer of PDMS (50 μm, Base : Curing Agent = 20:1, Sylagard 184 silicon elastomer, Dow Corning) was spin-coated onto a carrier glass substrate and thermally cured at 130 °C to provide a weak adhesive interface. The PET substrate (12 μm) was cleaned with ethanol, isopropyl alcohol, and DI water in sequence. After the PET substrate was dried in a 50 °C oven and cooled down to room temperature, it was transferred and carefully attached to the PDMS layer without air cavities.

Fabrication of encapsulation layer on PET substrate

The encapsulation layer of a 3.5 dyad organic-inorganic hybrid nano-stratified layer[53] was formed by a series of thermal ALD and spin-coating processes. In detail, an inorganic nano-stratified barrier was deposited by thermal ALD, composed of five repeating pairs of a 3 nm Al_2O_3 layer and a 3 nm ZnO layer. Al_2O_3 was formed using trimethylaluminum (TMA) and H_2O, and ZnO using diethylzinc (DEZ) and H_2O in a 70 °C chamber. A SiO_2-polymer composite (i-OPTO BC 10, INTECH Nano Materials Co., Ltd, Korea) was used as an organic layer. The organic layer was spin-coated and thermally cured at 70 °C for 20 min to form a 300 nm thick layer. The bottom encapsulation layer was formed on the PET substrate prior to the OLED deposition process, and the top layer was formed after the OLED deposition process. A layer of Kapton tape was attached to the end part of the electrode before the top encapsulation process and detached after, so that the active contact area for FFC cable connection is exposed.

Fabrication of OLEDs on PET substrate

The bottom-emitting OLEDs were fabricated on the bottom encapsulated PET substrate by thermal evaporation. The red OLEDs are fabricated with the following structure: Ag (30 nm)/MoO_3 (5 nm)/NPB (65 nm)/$Bebq_2$:$Ir(piq)_3$ (70 nm, 8 wt%)/Liq (1 nm)/Al (100 nm). The Ag was deposited as a transparent anode and MoO_3 as a hole injection layer. N, N0 diphenyl-N, N0-bis (1,10-biphenyl)-4,40-diamine (NPB) was used as a hole-transporting layer. The host material bis(10-hydroxybenzo(h)quinolinato)beryllium complex ($Bebq_2$) and the red emission dopant tris(1-phenylisoquinoline)iridium ($Ir(piq)_3$) were co-deposited for an emitting layer. 8-quinolinolato-lithium (Liq) was used as an electron injection layer, and Al as a cathode. The green OLEDs consisted of the following layers: Ag (30 nm)/MoO_3 (5 nm)/NPB (50 nm)/Alq_3 (50 nm)/Liq (1 nm)/Al (100 nm). Tris(8-hydroxyquinolinato)aluminum (Alq_3) was used as the green-emitting layer in the green OLEDs. The blue OLEDs had the following composition: Ag (25 nm)/MoO_3 (5 nm)/NPB (45 nm)/MADN:DSA-Ph (25 nm, 3 wt%)/Alq_3(10 nm)/Liq (1 nm)/ Al (100 nm). In the case of the blue OLEDs, the host material 2-methyl-9,10-di(2-naphthyl) anthracene (MADN) and the blue emission dopant p-bis(p-N,N-di-phenyl-aminostyryl) (DSA-Ph) were co-deposited to form the emitting layer, while Alq_3 was utilized as an electron transport layer.

Lamination and patterning process of the stretchable OLEDs

After the OLEDs were fabricated and fully encapsulated, an attachable PET film (12 μm film coated with a 6.5 μm-thick acrylic adhesive) was applied by a lamination process to protect the device from physical damage and moisture.

Table 1 | The table compares the SOLED of this work with previous SOLEDs, exhibiting its enhanced stretchability and effective electrode durability during stretching

Key Features Stretchable platform	Max. system strain (Max. electrode strain)	Stretch cycles (System strain)	Relative luminance after cyclic test	Water resistance	Emissive material	Operational lifetime	Luminance (Bias)	Max. current efficiency	Display array	Ref.
Hybrid platform Laser patterned Kirigami (PET)-islands on stress-relief pillar platform (PDMS)	95% (260%)	100,000 cycles (50%)	94%	1 month water storage, demonstrated	$Bebq_2$: $Ir(piq)_3$	753 h @ 1000 $cd{\cdot}m^{-2}$ (LT_{60}, Air)	6760 $cd{\cdot}m^{-2}$ (6.75 V)	15.7 $cd{\cdot}A^{-1}$	3 × 3	This Work
Hybrid platform Micro-cracked Au (SEBS) on stress-relief layer platform (SEBS)	30% 116%	1000 cycles (25%)	92%	-	NA	165 h @ 6000 $cd{\cdot}m^{-2}$ (LT_{95}, Air)	8510 $cd{\cdot}m^{-2}$ (5 V)	102 $cd{\cdot}A^{-1}$	17 × 7	[44]
Hybrid platform Photo-patterned serpentine(SU-8)-islands on stress-relief bilayer (Silbione-PDMS)	40% (140%)	1000 cycles (40%)	80%	-	Alq_3	-	3000 $cd{\cdot}m^{-2}$ (6.5 V)	EQE 2%	Single	[43]
Hybrid platform Photo-patterned serpentine(SU-8)-islands on stress-relief pillar platform (PDMS)	35% (104%)	2000 cycles (20%)	81%	-	Alq_3	50 h @ 150 $cd{\cdot}m^{-2}$ (LT_{50}, 50% duty, Air)	2000 $cd{\cdot}m^{-2}$ (7.5 V)	3 $cd{\cdot}A^{-1}$	Single	[42]
Pre-stretched platform Random wrinkles (NOA63/SiO2 NPs) on adhesive elastomer (3 M VHB 4905)	100% (Areal strain, EML-electrode combined)	100 cycles (30%; areal strain)	79%	Demonstrated	CBP: $Ir(ppy)_2tmd$	2.5 h @ 10,000 $cd{\cdot}m^{-2}$ (LT_{50})	Larger than 10,000 $cd{\cdot}m^{-2}$ (5 V)	82.4 $cd{\cdot}A^{-1}$	Single	[40]
Pre-stretched platform Micro-wrinkles controlled by pre-strained substrate (PDMS)	20% (EML-electrode combined)	1000 cycles (10%)	16%	-	SY	-	8000 $cd{\cdot}m^{-2}$ (10 V)	7.76 $cd{\cdot}A^{-1}$	4 × 4	[41]
Pre-stretched platform Periodic buckles (NOA63) on adhesive elastomer (3 M VHB 4905)	100% (EML-electrode combined)	35,000 cycles (20%)	73%	-	mCP: $Ir(ppy)_3$	-	15,110 $cd{\cdot}m^{-2}$ (6.5 V)	66 $cd{\cdot}A^{-1}$	Single	[39]
Pre-stretched platform Periodic buckles (NOA63) on adhesive elastomer (3 M VHB 4905)	100% (EML-electrode combined)	20,000 cycles (20%)	120%	-	CBP: $Ir(BT)_2(acac)$	-	20,000 $cd{\cdot}m^{-2}$ (7.5 V)	71 $cd{\cdot}A^{-1}$	5 × 1	[71]
Pre-stretched platform Random wrinkles (parylene) on silicone rubber (EcoFlex 00–30)	200% (EML-electrode combined)	1000 cycles (60%)	90%	-	NA	29 h (LT_{50})	4900 $cd{\cdot}m^{-2}$ (7.8 V)	53.7 $cd{\cdot}A^{-1}$	Single	[72]
Pre-stretched platform Periodic buckles (NOA63) on adhesive elastomer (3 M VHB 4905)	70% (EML-electrode combined)	15,000 cycles (20%)	~95%	-	mCP: $Ir(ppy)_3$	-	2200 $cd{\cdot}m^{-2}$ (7 V)	71 $cd{\cdot}A^{-1}$	Single	[73]
Pre-stretched platform Random buckles (NOA63) on adhesive elastomer (3 M VHB 4905)	80% (EML-electrode combined)	1000 cycles (40%)	NA	-	mCP: $Ir(ppy)_3$	-	9699 $cd{\cdot}m^{-2}$ (6.5 V)	79 $cd{\cdot}A^{-1}$	Single	[74]
Pre-stretched platform Random wrinkles (NOA63) on adhesive elastomer (3 M VHB 4905)	100% (EML-electrode combined)	2 cycles (100%)	NA	-	AnE-Pvstat	-	113 $cd{\cdot}m^{-2}$ (9 V)	0.026 $cd{\cdot}A^{-1}$	Single	[75]
Intrinsically stretchable Polymer chain engineered PLED	806% (EML-electrode combined)	-	NA	-	SBSPy-n	-	3274 $cd{\cdot}m^{-2}$ (28.5 V)	5.23 $cd{\cdot}A^{-1}$	Single	[76]
Intrinsically stretchable 3D nanonetwork PLED	40% (EML-electrode combined)	50 cycles (15%)	77%	-	L-SY-PPV/ PAN	-	3780 $cd{\cdot}m^{-2}$ (13 V)	8.13 $cd{\cdot}A^{-1}$	Single	[77]

Table 1 (continued) | The table compares the SOLED of this work with previous SOLEDs, exhibiting its enhanced stretchability and effective electrode durability during stretching

Key Features Stretchable platform	Max. system strain (Max. electrode strain)	Stretch cycles (System strain)	Relative luminance after cyclic test	Water resistance	Emissive material	Operational lifetime	Luminance (Bias)	Max. current efficiency	Display array	Ref.
Intrinsically stretchable AMOLEC enabled by inkjet printed OTFT	30% (EML-electrode combined)	20 cycles (30%)	NA	-	SY	-	-	NA	2 × 3	[35]
Intrinsically stretchable OLEC, electrode of AgNW soldered by GO	130% (EML-electrode combined)	100 cycles (40%)	40%	-	SY:OXD-7	-	1100 cd·m^{-2} (21 V)	2 cd·A^{-1}	Single	[78]
Intrinsically stretchable OLEC, AgNW on PUA substrate	120% (EML-electrode combined)	-	-	-	SY	10 h @ 211 cd·m^{-2} (LT_{50})	2200 cd·m^{-2} (21 V)	5.7 cd·A^{-1}	5 × 5	[79]
Intrinsically stretchable OLEC, CNT on PtBA substrate	45% (EML-electrode combined)	-	-	-	PF-B	7 h @ 170 cd·m^{-2} (LT_{55})	200 cd·m^{-2} (10 V)	1.24 cd·A^{-1}	Single	[80]

Unlike earlier studies, this work presents quantified water resistance performance and a water-proof 3 × 3 display demonstration. The SOLED also demonstrates consistent performance, luminance, and efficiency in ambient air.

Then, the whole device was lifted off from the carrier glass. The OLED device was patterned into a Kirigami-inspired island-interconnection structure by a laser cutting process using a Universal VLS 3.50 CO_2 laser cutter, with the laser path programmed through a computer-aided design program (AutoCAD, Autodesk Inc.) The interconnection structure was patterned with an optimized laser irradiation of 3.2 W, 350 PPI, and a travel speed of 200 mm/s.

Device characterization

For device characterization, the OLEDs were voltage-driven by a source meter (Keithley 2400, Keithley Inc.), which also measured the current. The corresponding electroluminescence and wavelength spectra of the devices were measured by a spectro-radiometer (CS-2000, Konica Minolta Inc.). The operational lifetime in air (23 ± 2 °C, 50 ± 10% RH) was measured by a lifetime measurement station using Si photodiodes (Polarnix M9000S, McScience Inc.). The mechanical stretching test was driven by a uni-axis stretching machine (ST1 Corp.).

Fabrication of a PDMS stress-relief pillar platform

The PDMS stress-relief pillar platform was fabricated by molding. The mold was processed by CNC machining circular holes of 1.5 mm diameter and 2.5 mm depth on a 4 mm thick aluminum plate. Each array is arranged at a pitch of 12 mm and consists of four cylindrical holes with 2.5 mm spacing. Then, the (heptadecafluoro-1,1,2,2-tetrahydrodecyl)trichlorosilane (JSI silicone) was coated on the mold by vaporization in a vacuum chamber for facile peel-off of the PDMS substrate. A PDMS solution (Sylagard 184 silicon elastomer, Dow Corning) with a mixing ratio of 20:1 (Base: Curing Agent) was cast on the mold, degassed in a vacuum chamber for 2 h, and spin-coated at 150 rpm for 10 s to achieve a 400 μm thickness. The cast PDMS solution was cured on a 130 °C hot plate for 30 min and preserved in a vacuum chamber for 1 day before peeling off.

Assembly of the SOLED display module

A thin layer of silicone adhesive is applied onto a carrier glass by knife-coating and then transferred to the tips of the pillars. The patterned SOLED is then transferred onto the pillar platform so the islands are attached to the pillar arrays. The entire structure was stored in a 70 °C oven for 30 min to set the SOLED to the stress-relief pillar platform permanently. The illustration for the fabrication procedure is presented in Supplementary Fig. 12.

Data availability

The data that support the findings of this study are available from the corresponding author upon reasonable request.

Received: 11 September 2023; Accepted: 24 February 2024;
Published online: 09 March 2024

References

1. Matsuhisa, N., Chen, X., Bao, Z. & Someya, T. Materials and structural designs of stretchable conductors. *Chem. Soc. Rev.* **48**, 2946–2966 (2019).
2. Dai, Y., Hu, H., Wang, M., Xu, J. & Wang, S. Stretchable transistors and functional circuits for human-integrated electronics. *Nat. Electron.* **4**, 17–29 (2021).
3. Heng, W., Solomon, S. & Gao, W. Flexible electronics and devices as human–machine interfaces for medical robotics. *Adv. Mater.* **34**, 2107902 (2022).
4. Jiang, S. et al. Flexible metamaterial electronics. *Adv. Mater.* **34**, 2200070 (2022).
5. Liu, S., Rao, Y., Jang, H., Tan, P. & Lu, N. Strategies for body-conformable electronics. *Matter* **5**, 1104–1136 (2022).
6. Liu, K., Ouyang, B., Guo, X., Guo, Y. & Liu, Y. Advances in flexible organic field-effect transistors and their applications for flexible electronics. *npj Flex.* **6**, 1 (2022).
7. Zhang, Z. Light-emitting materials for wearable electronics. *Nat. Rev. Mater.* **7**, 839–840 (2022).

8. Yao, L. Q. et al. High-efficiency stretchable organic light-emitting diodes based on ultra-flexible printed embedded metal composite electrodes. *InfoMat* **5**, e12410 (2023).
9. Yi, N. et al. Fabricating functional circuits on 3D freeform surfaces via intense pulsed light-induced zinc mass transfer. *Mater. Today* **50**, 24–34 (2021).
10. Zhang, W., Zhang, L., Liao, Y. & Cheng, H. Conformal manufacturing of soft deformable sensors on the curved surface. *Int J. Extrem. Manuf.* **3**, 042001 (2021).
11. Wu, H. et al. Fabrication techniques for curved electronics on arbitrary surfaces. *Adv. Mater. Technol.* **5**, 2000093 (2020).
12. Yin, H., Zhu, Y., Youssef, K., Yu, Z. & Pei, Q. Structures and materials in stretchable electroluminescent devices. *Adv. Mater.* **34**, 2106184 (2022).
13. Zheng, B., Zhao, G., Yan, Z., Xie, Y. & Lin, J. Direct freeform laser fabrication of 3D conformable electronics. *Adv. Funct. Mater.* **33**, 2210084 (2023).
14. Wan, Y. et al. Stretchable and self-healing elastomers with aggregation-induced emission based on hydrogen bonding cross-linked networks. *Macromolecules* **56**, 3345–3353 (2023).
15. Liu, C. et al. Wavelength-tunable organic semiconductor lasers based on elastic distributed feedback gratings. *J. Semicond.* **44**, 032601 (2023).
16. Koo, J. H., Kim, D. C., Shim, H. J., Kim, T. H. & Kim, D. H. Flexible and stretchable smart display: materials, fabrication, device design, and system integration. *Adv. Funct. Mater.* **28**, 1801834 (2018).
17. Lee, S. M., Kwon, J. H., Kwon, S. & Choi, K. C. A review of flexible OLEDs toward highly durable unusual displays. *IEEE Trans. Electron. Devices* **64**, 1922–1931 (2017).
18. Jeong, E. G., Kwon, J. H., Kang, K. S., Jeong, S. Y. & Choi, K. C. A review of highly reliable flexible encapsulation technologies towards rollable and foldable OLEDs. *J. Inf. Disp.* **21**, 19–32 (2020).
19. Lee, H. et al. Stretchable organic optoelectronic devices: design of materials, structures, and applications. *Mater. Sci. Eng. R. Rep.* **146**, 100631 (2021).
20. Heo, J. S., Eom, J., Kim, Y. H. & Park, S. K. Recent progress of textile-based wearable electronics: a comprehensive review of materials, devices, and applications. *Small* **14**, 1703034 (2018).
21. Baeg, K. J. & Lee, J. Flexible electronic systems on plastic substrates and textiles for smart wearable technologies. *Adv. Mater. Technol.* **5**, 2000071 (2020).
22. Song, J., Lee, H., Jeong, E. G., Choi, K. C. & Yoo, S. Organic light-emitting diodes: pushing toward the limits and beyond. *Adv. Mater.* **32**, 1907539 (2020).
23. Kwon, S. et al. Recent progress of fiber shaped lighting devices for smart display applications—a fibertronic perspective. *Adv. Mater.* **32**, 1903488 (2020).
24. Hwang, Y. H. et al. Organic light-emitting fibers and fabrics for truly wearable smart displays: recent progress and future opportunities. *J. Soc. Inf. Disp.* **30**, 727–747 (2022).
25. Shi, X. et al. Large-area display textiles integrated with functional systems. *Nature* **591**, 240–245 (2021).
26. Trung, T. Q. & Lee, N. E. Flexible and stretchable physical sensor integrated platforms for wearable human-activity monitoringand personal healthcare. *Adv. Mater.* **28**, 4338–4372 (2016).
27. Cho, H. et al. Recent progress in strain-engineered elastic platforms for stretchable thin-film devices. *Mater. Horiz.* **9**, 2053–2075 (2022).
28. Obropta, E. E. & Newman, D. J. A comparison of human skin strain fields of the elbow joint for mechanical counter pressure space suit development. In *Proc. IEEE Aerosp Conf* 1–9 (IEEE, 2015).
29. Matsuda, R. et al. Highly stretchable sensing array for independent detection of pressure and strain exploiting structural and resistive control. *Sci. Rep.* **10**, 12666 (2020).
30. Hwang Lee, G. et al. Stretchable PPG sensor with light polarization for physical activity-permissible monitoring. *Sci. Adv.* **8**, 3622 (2022).
31. Kwon, J. H. et al. Design of highly water resistant, impermeable, and flexible thin-film encapsulation based on inorganic/organic hybrid layers. *ACS Appl Mater. Interfaces* **11**, 3251–3261 (2019).
32. Jeong, S. Y. et al. Foldable and washable textile-based OLEDs with a multi-functional near-room-temperature encapsulation layer for smart e-textiles. *npj Flex.* **5**, 15 (2021).
33. Jeong, S. Y. et al. Highly air-stable, flexible, and water-resistive 2D titanium carbide mxene-based RGB organic light-emitting diode displays for transparent free-form electronics. *ACS Nano* https://doi.org/10.1021/acsnano.3c00781 (2023).
34. Liang, J. et al. Intrinsically stretchable and transparent thin-film transistors based on printable silver nanowires, carbon nanotubes and an elastomeric dielectric. *Nat. Commun.* **6**, 7647 (2015).
35. Liu, J. et al. Fully stretchable active-matrix organic light-emitting electrochemical cell array. *Nat. Commun.* **11**, 3362 (2020).
36. Kim, J.-H. & Park, J.-W. Intrinsically stretchable organic light-emitting diodes. *Sci. Adv.* **7**, eabd9715 (2021).
37. Zhao, Z., Liu, K., Liu, Y., Guo, Y. & Liu, Y. Intrinsically flexible displays: key materials and devices. *Natl Sci. Rev.* **9**, nwac090 (2022).
38. Hafeez, H. et al. Multiaxial wavy top-emission organic light-emitting diodes on thermally prestrained elastomeric substrates. *Org. Electron* **48**, 314–322 (2017).
39. Yin, D. et al. Roller-assisted adhesion imprinting for high-throughput manufacturing of wearable and stretchable organic light-emitting devices. *Adv. Opt. Mater.* **8**, 1901525 (2020).
40. Choi, D. K. et al. Highly efficient, heat dissipating, stretchable organic light-emitting diodes based on a MoO3/Au/MoO3 electrode with encapsulation. *Nat. Commun.* **12**, 2864 (2021).
41. Jeong, S., Yoon, H., Lee, B., Lee, S. & Hong, Y. Distortion-free stretchable light-emitting diodes via imperceptible microwrinkles. *Adv. Mater. Technol.* **5**, 2000231 (2020).
42. Lim, M. S. et al. Two-dimensionally stretchable organic light-emitting diode with elastic pillar arrays for stress relief. *Nano Lett.* **20**, 1526–1535 (2020).
43. Kim, T., Lee, H., Jo, W., Kim, T. S. & Yoo, S. Realizing stretchable OLEDs: a hybrid platform based on rigid island arrays on a stress-relieving bilayer structure. *Adv. Mater. Technol.* **5**, 2000494 (2020).
44. Lee, Y. et al. Standalone real-time health monitoring patch based on a stretchable organic optoelectronic system. *Sci. Adv.* **7**, eabg9180 (2021).
45. Zhang, X., Yu, Q., Wu, H. & Cheng, H. Controlled bi-axial buckling and postbuckling of thin films suspended on a stretchable substrate with square prism relief structures. *Int J. Appl Mech.* **14**, 2150123 (2022).
46. Hanif, A. et al. A skin-inspired substrate with spaghetti-like multi-nanofiber network of stiff and elastic components for stretchable electronics. *Adv. Funct. Mater.* **30**, 2003540 (2020).
47. Shyu, T. C. et al. A kirigami approach to engineering elasticity in nanocomposites through patterned defects. *Nat. Mater.* **14**, 785–789 (2015).
48. Jang, B. et al. Auxetic meta-display: stretchable display without image distortion. *Adv. Funct. Mater.* **32**, 2113299 (2022).
49. Yin, L., Lv, J. & Wang, J. Structural innovations in printed, flexible, and stretchable electronics. *Adv. Mater. Technol.* **5**, 2000694 (2020).
50. Kim, D. C. et al. Three-dimensional foldable quantum dot light-emitting diodes. *Nat. Electron* **4**, 671–680 (2021).
51. Hecht, D. S., Hu, L. & Irvin, G. Emerging transparent electrodes based on thin films of carbon nanotubes, graphene, and metallic nanostructures. *Adv. Mater.* **23**, 1482–1513 (2011).
52. Jeon, Y., Lee, H., Kim, H. & Kwon, J. H. A review of various attempts on multi-functional encapsulation technologies for the reliability of OLEDs. *Micromachines* **13**, 1478 (2022).
53. Jeong, E. G. et al. A mechanically enhanced hybrid nano-stratified barrier with a defect suppression mechanism for highly reliable flexible OLEDs. *Nanoscale* **9**, 6370–6379 (2017).

54. Jeong, E. G., Jeon, Y., Cho, S. H. & Choi, K. C. Textile-based washable polymer solar cells for optoelectronic modules: toward self-powered smart clothing. *Energy Environ. Sci.* **12**, 1878–1889 (2019).
55. Won, P. et al. Stretchable and transparent kirigami conductor of nanowire percolation network for electronic skin applications. *Nano Lett.* **19**, 6087–6096 (2019).
56. Xue, Z., Song, H., Rogers, J. A., Zhang, Y. & Huang, Y. Mechanically-guided structural designs in stretchable inorganic electronics. *Adv. Mater.* **32**, 1902254 (2020).
57. Forrest, S. R. The path to ubiquitous and low-cost organic electronic appliances on plastic. *Nature* **428**, 911–918 (2004).
58. Lee, H. C., Hsieh, E. Y., Yong, K. & Nam, S. W. Multiaxially-stretchable kirigami-patterned mesh design for graphene sensor devices. *Nano Res* **13**, 1406–1412 (2020).
59. Zhang, Z., Tian, Z., Mei, Y. & Di, Z. Shaping and structuring 2D materials via kirigami and origami. *Mater. Sci. Eng. R. Rep.* **145**, 100621 (2021).
60. Choi, H. et al. Highly stretchable and strain-insensitive liquid metal based elastic kirigami electrodes (LM-eKE). *Adv. Funct. Mater.* **33**, 2301388 (2023).
61. Yang, L. et al. Moisture-resistant, stretchable NOx gas sensors based on laser-induced graphene for environmental monitoring and breath analysis. *Microsyst. Nanoeng.* **8**, 78 (2022).
62. Zhang, C. et al. Laser processing of crumpled porous graphene/mxene nanocomposites for a standalone gas sensing system. *Nano Lett.* **23**, 3435–3443 (2023).
63. Yang, L. et al. Self-healing, reconfigurable, thermal-switching, transformative electronics for health monitoring. *Adv. Mater.* **35**, 2207742 (2023).
64. Xue, Y. et al. Superhydrophobic, stretchable kirigami pencil-on-paper multifunctional device platform. *Chem. Eng. J.* **465**, 142774 (2023).
65. Karami-Mosammam, M., Danninger, D., Schiller, D. & Kaltenbrunner, M. Stretchable and biodegradable batteries with high energy and power density. *Adv. Mater.* **34**, 2204457 (2022).
66. Amiri, A. et al. Fully integrated design of a stretchable kirigami-inspired micro-sized zinc-sulfur battery. *J. Mater. Chem. A Mater.* **11**, 10788–10797 (2023).
67. Snakenborg, D., Klank, H. & Kutter, J. P. Microstructure fabrication with a Co2 laser system. *J. Micromech. Microeng.* **14**, 182–189 (2004).
68. Takeuchi, T., De Valois, K. K. & Hardy, J. L. The influence of color on the perception of luminance motion. *Vis. Res* **43**, 1159–1175 (2003).
69. Choi, Y.-T. & Cho, R. A study on the method of OLED device's lifetime test. In *Proc Saf Manag Sci Conf* 131–143 (IEEE, 2008).
70. Blees, M. K. et al. Graphene kirigami. *Nature* **524**, 204–207 (2015).
71. Yin, D. et al. Mechanically robust stretchable organic optoelectronic devices built using a simple and universal stencil-pattern transferring technology. *Light Sci. Appl* **7**, 35 (2018).
72. Yokota, T. et al. Ultraflexible organic photonic skin. *Sci. Adv.* **2**, e1501856 (2016).
73. Yin, D. et al. Efficient and mechanically robust stretchable organic light-emitting devices by a laser-programmable buckling process. *Nat. Commun.* **7**, 11573 (2016).
74. Yin, D. et al. Two-dimensional stretchable organic light-emitting devices with high efficiency. *ACS Appl Mater. Interfaces* **8**, 31166–31171 (2016).
75. White, M. S. et al. Ultrathin, highly flexible and stretchable PLEDs. *Nat. Photonics* **7**, 811–816 (2013).
76. Li, X. C. et al. Intrinsically stretchable electroluminescent elastomers with self-confinement effect for highly efficient non-blended stretchable OLEDs. *Angew. Chem.* **135**, e202213749 (2023).
77. Liu, Y. et al. A self-assembled 3D penetrating nanonetwork for high-performance intrinsically stretchable polymer light-emitting diodes. *Adv. Mater.* **34**, 2201844 (2022).
78. Liang, J. et al. Silver nanowire percolation network soldered with graphene oxide at room temperature and its application for fully stretchable polymer light-emitting diodes. *ACS Nano* **8**, 1590–1600 (2014).
79. Liang, J., Li, L., Niu, X., Yu, Z. & Pei, Q. Elastomeric polymer light-emitting devices and displays. *Nat. Photonics* **7**, 817–824 (2013).
80. Yu, Z., Niu, X., Liu, Z. & Pei, Q. Intrinsically stretchable polymer light-emitting devices using carbon nanotube-polymer composite electrodes. *Adv. Mater.* **23**, 3989–3994 (2011).

Acknowledgements

This work was supported by the Technology Innovation Program (20017569, Development of substrate materials that can be stretched more than 50% for stretchable displays) funded by the Ministry of Trade, Industry & Energy (MOTIE, Korea) and the Engineering Research Center of Excellence (ERC) Program supported by the National Research Foundation (NRF), Korean Ministry of Science, ICT and Future Planning (MSIP) (NRF-2017R1A5A1014708). In addition, this work was also supported by project for materials, parts and equipment strategic cooperation R&D funded Korea Ministry of SMEs and Startups in 2022 (2022-00165409), and by the NRF funded by the MSIP (2022R1F1A1075914). We also would like to acknowledge the technical support from ANSYS Korea.

Competing interests

The authors declare no competing interests.

Additional information

Supplementary information The online version contains supplementary material available at https://doi.org/10.1038/s41528-024-00303-5.

Correspondence and requests for materials should be addressed to Jeong Hyun Kwon or Kyung Cheol Choi.